

Seasonal Variations in the Southern Hemisphere Storm Tracks and Associated Wave Propagation

V. BRAHMANANDA RAO, A. M. C. DO CARMO, AND SERGIO H. FRANCHITO

Centro de Previsão de Tempo e Estudos Climáticos, Instituto Nacional de Pesquisas Espaciais, São José dos Campos, São Paulo, Brazil

(Manuscript received 2 August 2000, in final form 24 July 2001)

ABSTRACT

Seasonal variations in the Southern Hemisphere (SH) storm track characteristics and associated wave propagation are studied using 19 years of NCEP–NCAR gridded data. It is found that the SH storm track is strongest in the austral autumn season and weakest in spring. The characteristics of wave packets are studied by computing 1-point lag correlation maps with unfiltered meridional wind at 300 hPa. It is found that the eastward group velocities of waves are much higher than the phase velocities in the transition seasons. This shows that the downstream development occurs throughout the year and is a basic feature of upper-tropospheric waves in the midlatitudes of the SH. This extends previous studies made for winter and summer seasons. Based on the indices that show wave coherence and correlation maps, it is found that the pathways in the transition seasons split into two branches east of Australia, in a way similar to what happens in the zonal wind distribution.

1. Introduction

Pioneering studies by Charney (1947) and Eady (1949) showed that the midlatitude westerlies are baroclinically unstable. Several subsequent investigations established that extratropical disturbances grow baroclinically extracting available potential energy from the meridional temperature gradient by transporting sensible heat poleward and converting available potential energy into kinetic energy by zonal and vertical thermally direct circulations. The concept of these energy exchanges evolved by considering a zonal mean flow and its deviations (Lorenz 1955). These ideas supported further theoretical studies that considered a zonal mean westerly current and a disturbance superimposed on that. The characteristics deduced from these theoretical studies, such as the most unstable wavelength and its vertical structure, seem to agree with the observed features.

In the middle and late 1970s a different methodology has been used to study the midlatitude disturbances (Blackmon 1976; Blackmon et al. 1977). Instead of a zonal mean and its deviation, a time mean and deviation are adopted. These observational studies have shown that synoptic disturbances are organized mainly into “storm tracks” situated slightly poleward and downstream of the positions of the middle-latitude mean jet maxima (Blackmon et al. 1977). Storm tracks are re-

gions where the variance of variables like geopotential and meridional wind is largest.

Although several investigations have been made to study storm tracks in the Northern Hemisphere (NH) (Blackmon et al. 1984a,b; Wallace et al. 1988; Lim and Wallace 1991), similar studies for Southern Hemisphere (SH) storm tracks are much smaller in number. Trenberth (1981, 1982) examined transients in the SH and their role in the momentum fluxes using analysis prepared by the World Meteorological Centre in Melbourne, Australia. Trenberth (1991) used 11 years of European Centre for Medium-Range Weather Forecasts (ECMWF) analysis to study the SH storm tracks. He found that the SH storm track is mostly zonally oriented along 50°S during all seasons. The variance of bandpass filtered (2- to 8-day period) variables is highest over the Indian Ocean and lowest in the eastern sector of the Pacific Ocean. Randel and Stanford (1985) showed that in the SH summer, medium-scale waves (wavenumbers 6–7) exhibit baroclinic life cycles similar to those of unstable normal modes in simplified numerical models. Randel and Held (1991) found that eastward-moving medium-scale waves (zonal wavenumbers 4–7) dominate the spectra of lower-tropospheric heat fluxes in both the hemispheres in all seasons. From these observations, Lee and Held (1993) inferred that the summer storm track is more oriented meridionally. This they suggested as favorable for higher wave coherence in summer since coherent eddies are generally easier to obtain when there is only one dimension in which the eddies can propagate. Using three-dimensional instability theory Frederiksen and Frederiksen (1993) showed that in the SH,

Corresponding author address: Dr. V. Brahmananda Rao, Instituto Nacional de Pesquisas Espaciais, 12201-970, São José dos Campos, SP, Brazil.
E-mail: vbrao@cptec.inpe.br

maximum amplitudes in January and July are located somewhat downstream of the regions of maximum observed baroclinicity.

Observational studies (e.g., Namias and Clapp 1944; Cressman 1948; Höymoeller 1949) for the NH and van Loon (1965) for the SH have shown that downstream development of baroclinic waves occurs in the mid- and upper troposphere. Simmons and Hoskins (1979) showed that downstream development of baroclinic waves occurs in nonlinear integrations of model simulation using a localized nonmodal perturbation as initial condition. Recently, Orlanski and Katzfey (1991), Chang (1993), Lee and Held (1993), Berbery and Vera (1996), Chang and Yu (1999), and Chang (1999) showed that baroclinic waves in the midlatitude storm tracks tend to be organized in localized wave packets that clearly exhibit downstream development. Chang (1993) and Berbery and Vera (1996) showed that time filtering can alter artificially the temporal evolution characteristics of wave packets and hence the use of unfiltered data is necessary.

Regarding the dynamics of downstream-developing wave packets, Orlanski and Katzfey (1991), Orlanski and Chang (1993), Chang and Orlanski (1993), and Chang (1993) found that growth of new perturbations toward the downstream side of existing waves is triggered by energy fluxes from existing upstream perturbations. Orlanski and Katzfey (1991) found that an eastward ageostrophic geopotential flux can provide the initial triggering mechanism for downstream development. This is different from the usual concept of life cycle of baroclinic waves in which the waves grow baroclinically and decay barotropically (Simmons and Hoskins 1978; Randel and Stanford 1985).

In his recent study of wave packets in the upper troposphere, Chang (1999, hereafter referred to as C99) documented the seasonal variations in both the hemispheres. However, he examined only summer and winter seasons. As we shall see later, the SH storm tracks (as given by the variance of unfiltered meridional wind) are strongest in austral autumn season and weakest in austral spring. This necessitates a study of storm tracks in all the four seasons. In a previous study, Trenberth (1991) also noted that the storm tracks in the SH are strongest in the austral autumn season. However, he defined storm tracks in terms of 2–8-day filtered standard deviation of geopotential height. Chang and Yu (1999) noted differences between storm tracks identified in geopotential height and meridional (nongeostrophic) wind data. For example, Chang and Yu (1999) did not find a break between the North Pacific and North Atlantic storm tracks. Such a break was noted in bandpass-filtered 500-hPa geopotential height data (e.g., Blackmon 1976). This is because winds in the eddies are strongly supergeostrophic over the western North America, such that the variance in total meridional wind does not display a significant minimum between the Pacific and Atlantic storm tracks (Lau 1978; Chang and Yu 1999). Also, as

pointed by Chang (1993) and Berbery and Vera (1996) time filtering can alter erroneously temporal evolution characteristics of wave packets. Thus, it would be necessary to reexamine the storm tracks in the SH with unfiltered meridional wind. In the present paper we extend the analysis of C99 by studying the characteristics of storm tracks and associated wave packets in the SH in all the four seasons giving emphasis to the transition seasons.

2. The data source and method of analysis

In the present study we use the gridded data from the National Centers for Environmental Prediction–National Center for Atmospheric Research (NCEP–NCAR) reanalysis for the period January 1979 through December 1997. Although data were available to us from 1973 onward, we restricted analysis from 1979 since satellite observations improved the reliability of data since 1979. We use daily 300-hPa meridional wind v . A detailed description of the NCEP–NCAR assimilation systems and output was given by Kalnay et al. (1996). Since time filtering can alter the temporal evolution characteristics of wave packets (Chang 1993; Berbery and Vera 1996), we use in this study unfiltered data. Data are given on a 2.5° latitude \times 2.5° longitude grid. Since we are interested in transient waves, we removed the stationary component by subtracting long period monthly mean from individual daily values. This is represented by v' . Assuming a simple wave function for v' , $v' = A \sin \omega t$, it can be shown that $\overline{v'^2} = A^2/2$, where the overbar is a time mean over one period. Thus the instantaneous amplitude of v' is represented as the square root of the envelope function, after multiplying the squared time series of v' by a factor of 2. Since the (square rooted) envelope function represents a local, instantaneous amplitude of the fluctuations in v' , it should be a good measure of the local amplitude (or activity) of baroclinic waves. This we represent by v_e . This method of obtaining v_e is essentially the same as the one used by Nakamura and Wallace (1990) except that they used filtered geopotential height data.

3. Results

a. Storm tracks in the transition seasons

Figure 1 shows the standard deviation of the meridional component of wind ($\sqrt{v'^2}$) for each of the four seasons. The maximum (shading corresponds to more than 14 m s^{-1}) corresponds to the midlatitudes storm tracks, which vary both in the strength and shape in all the four seasons. The SH storm track is strongest and most extensive in austral autumn [March, April, and May (MAM)] with the largest extension of values 16 m s^{-1} or more. In this season, the storm track covers the entire SH around 50°S except for a small region in the Atlantic near the tip of South America. The storm

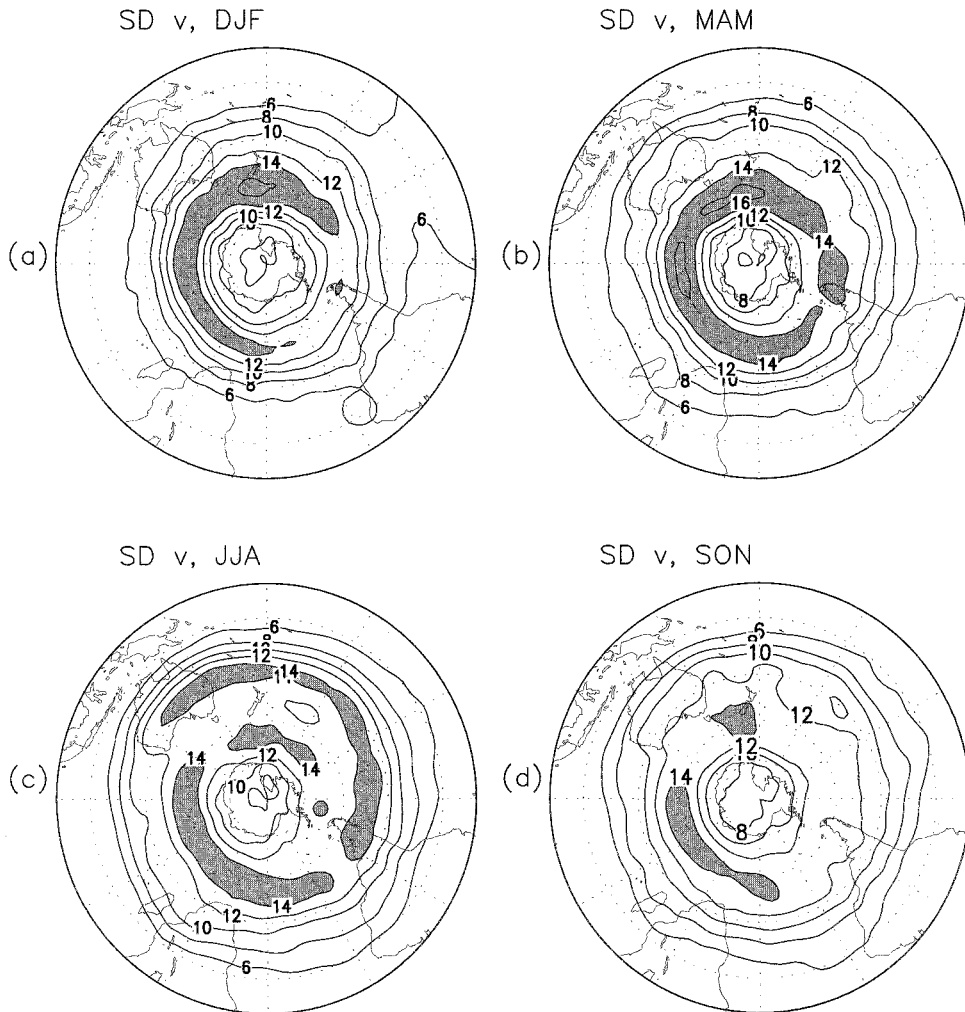


FIG. 1. Standard deviation of 300-hPa v' . Contour intervals are 2 m s^{-1} . Shaded areas denote values greater than 14 m s^{-1} .

track is weakest and least extensive in austral spring [September, October, and November (SON)]. During austral winter [June, July, and August (JJA)] the storm track shows a spiral around the SH, starting over Australia, running across the Pacific, South America, and Southern Atlantic, passing south of Africa and the south Indian Ocean and then running south of Australia and New Zealand to farther south of the northern storm track starting over Australia. Such a spiral can also be seen in C99 and Berbery and Vera's (1996) standard deviation in relative vorticity. In Fig. 1c because of polar stereographic projection, however, the spiral is better defined. Compared to the values of standard deviation of meridional wind in C99, his Fig. 2, our values are slightly lower. Chang (2000) showed that the SH storm tracks are stronger in the ECMWF reanalysis than in the NCEP-NCAR reanalysis.

Comparing Fig. 1 with the figure for the standard deviation of v_e (figure not shown), we see that characteristics of the storm tracks are similar except that the

storm track is smoother. Again, we see that the storm track in autumn is strongest. The spiral in winter seasons is also clearly seen.

In order to see clearly the monthly variation, Fig. 2a is prepared. Mean v_e for $45^\circ\text{--}55^\circ\text{S}$ for each longitude is shown. From Fig. 1 it can be seen that the principal storm track is between 45° and 55°S in all 12 months, although in winter an additional branch of storm track is seen at $20^\circ\text{--}30^\circ\text{S}$ between the longitudes 150° and 90°W . Thus the average between 45° and 55°S will take into account the small seasonal migration of the principal storm track. In Fig. 2a the isolines of v_e are smoothed using a 31-day running average along the time (y) axis and a 5-point average along the x axis. At the 300-hPa level the baroclinic activity is most dominant in the beginning of April (as given by 19 m s^{-1} contour). The values of v_e start increasing from around the end of October reaching a maximum in April. In order to see the effect of taking average over a broader latitude band, we prepared Fig. 2a taking the average over 40°--

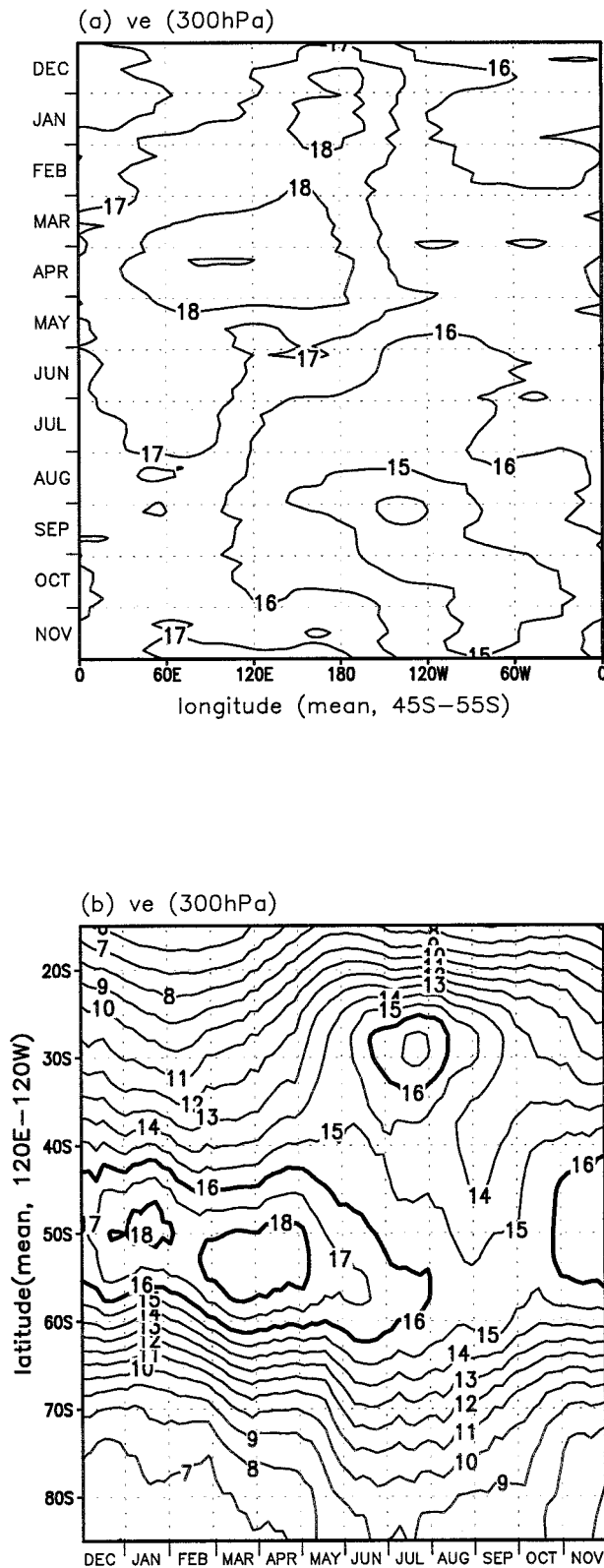


FIG. 2. (a) Time-longitude section of v_e . The isolines of v_e are smoothed using a 31-day running average along the time (y axis) and a 5-point average along the longitude (x axis). (b) Time-latitude section of v_e . Contour interval: 1 m s^{-1} .

60°S latitude band. This figure (not shown) confirms that the storm track is weakest in October and strongest in April.

Figure 2b shows the time-latitude section of wave amplitude based on zonal average over 120°E – 120°W . The seasonal migration of the storm track (as given by 15 m s^{-1} contour) clearly shows an equatorward penetration in winter starting in the beginning of June. This subtropical storm track starts weakening from the middle of August. In winter months two branches of storm tracks, one around 27°S and the other around 55°S , can be seen (see Fig. 1 for a hemispheric view). In this figure (Fig. 2b) also the storm track is strongest (as given by 18 m s^{-1} contour) and widest in the austral autumn season.

Figure 3 shows the distribution of mean (of 19 years) zonal wind for transition seasons at 300 hPa. The characteristics of mean zonal wind for December, January, and February (DJF) and JJA (figure not shown) are similar to those noted in C99. Particularly, noteworthy features are the zonally symmetric distribution of the westerly jet in DJF and a split in the jet in JJA associated with poleward spiral starting at about 30°S over the Indian Ocean (60°E) and returning to the same longitude at a higher latitude. The split jet occurs also in SON and MAM (Fig. 3). Later, while discussing the characteristics of the wave propagation for the transition seasons (section 3d), we found that the wave train appears to split into two branches to the east of Australia propagating along the subtropical and subpolar jets in SON and MAM in a way similar to what was noted for JJA in C99.

b. Characteristics of the waves and wave packets

We obtained the characteristics of wave packets by computing 1-point lag correlation maps. These maps are obtained by calculating the correlation of time series of 300-hPa v' at each grid point on a $2.5^\circ \times 2.5^\circ$ grid between 10° and 70°S with time series of 300 hPa v' at every other grid point in the SH. At lag 0 these maps show a wave train extending generally along the latitude circles, showing centers of positive and negative correlations. Based on these maps, we can estimate the dominant wavelength of the waves at each location. The characteristic phase speed of waves picked out by correlation analysis can be estimated by tracking the movement of the maximum positive center from day -1 and day $+1$. The characteristic period of waves can be found by dividing the wavelength by the phase speed. Based on this methodology the characteristic wavelength, phase speed, and period are calculated for all the seasons in the SH. However, we present here the characteristics of waves in the transition seasons since results for summer and winter seasons are nearly similar to those obtained by C99.

The results of wavelength are displayed in terms of wave numbers (figure not shown). At about 50°S , the main latitude of storm track, the dominant wavenumber is around 5–6 in both the transition seasons. The wavenumbers seem to decrease toward higher latitudes in

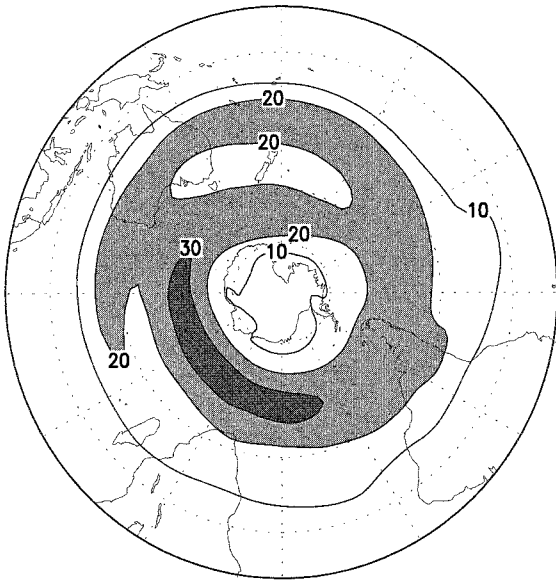
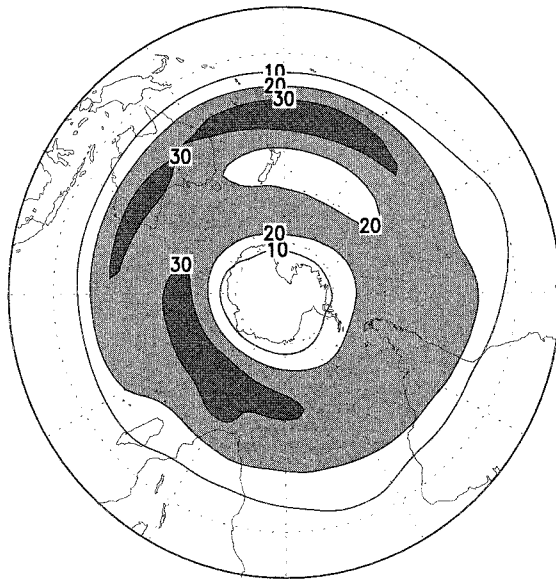
(a) \bar{U}_{bar} (300 hPa), MAM(b) \bar{U}_{bar} (300 hPa), SON

FIG. 3. Mean zonal wind (m s^{-1}) at 300 hPa for the transition seasons. Shading corresponds to values greater than 20 m s^{-1} .

both the transition seasons. In both the transition seasons the dominant wavenumber increases toward lower latitudes reaching 7–8 at 30°S and then decreases toward the equator. This is a little different than what happens in summer (Fig. 3a of C99) when the wavenumbers in the lower latitudes seem to be slightly higher. In both winter and summer seasons (Fig. 3c of C99) the wavenumbers in the high latitudes of the SH are somewhat higher compared to the transition seasons.

It would be interesting to obtain the phase velocity that can be compared with group velocities. The phase speed is eastward in all seasons except in summer (figure not shown) near the equator where it is less than 2 m s^{-1} or negative. In both the transition seasons a band of high phase velocities (around 10 m s^{-1}) is seen around 50°S over the Indian Ocean. This value (10 m s^{-1}) is somewhat less than that obtained by C99 for summer and winter seasons (his Fig. 4). The characteristic period of the waves lies between 3 and 8 days in all the seasons between 20° and 65°S .

The group velocity of the wave packets is determined by objectively tracking the movement of the centers of correlation obtained with v_c from day -1 to day $+1$. A comparison of zonal phase and group velocities shows that group velocity is much higher than phase velocity in all the seasons (figures not shown). Thus the downstream development occurs in all seasons. The meridional group velocity (figure not shown) is equatorward on the equatorward side of the storm track and poleward on the poleward side, indicating divergence of wave energy away from the storm tracks. The features found in DJF and JJA agree in general with those of C99, and here we extended his study to other seasons also pointing out the differences and similarities.

c. Characteristics of seasonal variations in wave propagation coherence

To obtain the relative importance of downstream and upstream development, downstream–upstream asymmetry index is calculated. Figure 4 shows the downstream–upstream asymmetry index for the transition seasons. This index is equal to the sum of the maximum negative correlation upstream at day -1 and that downstream at day $+1$ divided by the sum of maximum downstream negative correlation at day -1 and upstream correlation at day $+1$. A ratio greater than 1 indicates that the downstream development occurs, whereas values smaller than 1 indicate upstream development and values close to 1 indicate that the waves are simply advected by the steering flow (C99). In Fig. 4 it can be seen that in all the transition seasons the index is more than 1 over most regions indicating the occurrence of downstream development. Results of C99 and our results (figure not shown) show that downstream development occurs also in summer and winter seasons. This suggests that downstream development occurs over most regions in all the four seasons.

In order to see wave coherence, the wave coherence index (Fig. 5) is calculated for the transition seasons. This is the average of the maximum (positive or negative) correlation upstream on day -2 and the downstream on day $+2$. This index indicates how well the waves in each location correlate with upstream waves 2 days earlier and downstream waves 2 days later, thus showing the tendency of downstream development of waves. Highest index (0.55) occurs in summer (figure

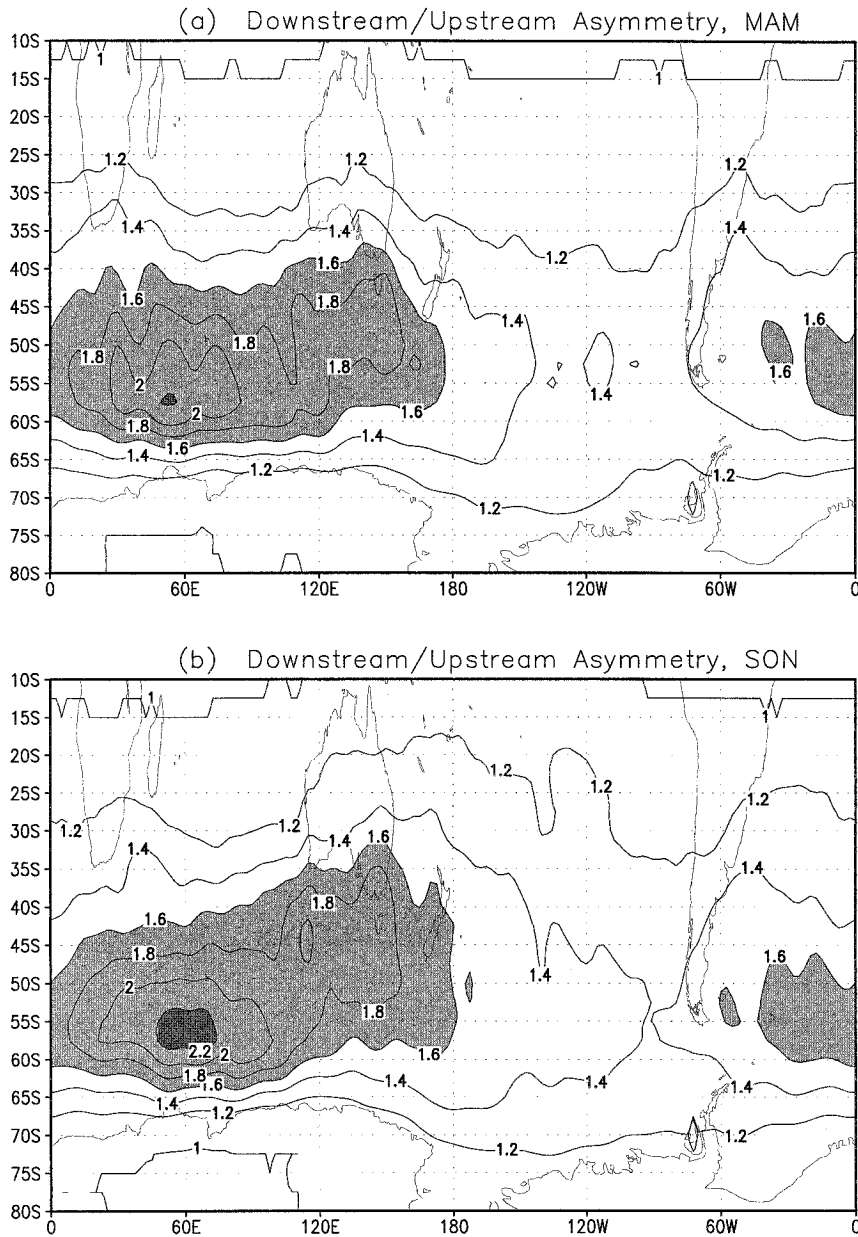


FIG. 4. Downstream-upstream asymmetry index. Contour interval: 0.2. Shading represents values greater than 1.6.

not shown) over the south Indian Ocean around 50°E and 50°S and zonal symmetry is high in this season. This is similar to what C99 noted. A characteristic not noted by C99 is that in summer a region of high coherence is seen on the eastern Pacific near 10° – 15°S and continues to the west coast of South America. This suggests that there are coherent disturbances travelling westward (because of the easterlies) in this region.

In autumn (Fig. 5a) when the storm track is most intense, the wave coherence is zonally most extensive around 50°S with values of 0.5 or more. Our values seem to be a little higher than those of C99 for summer

and winter. Also in autumn (Fig. 5a) the band of 0.5 extends over a substantially larger latitudinal band to the east Australia around 180° . In spring (Fig. 5b) also around 50°S there is a zonal band of 0.5 with a break from 150°E to 180° . To the east of 180° the zone of high coherence (values ≥ 0.5) is meridionally more extensive. This is similar to what happens in winter. In winter (see Fig. 9b of C99) a band of high coherence occurs between 45° – 65°S in the south Indian Ocean and east of this region around 120°E the band appears to split into two regions of high coherence with lower values in between. As we shall see later (section 3d), indeed

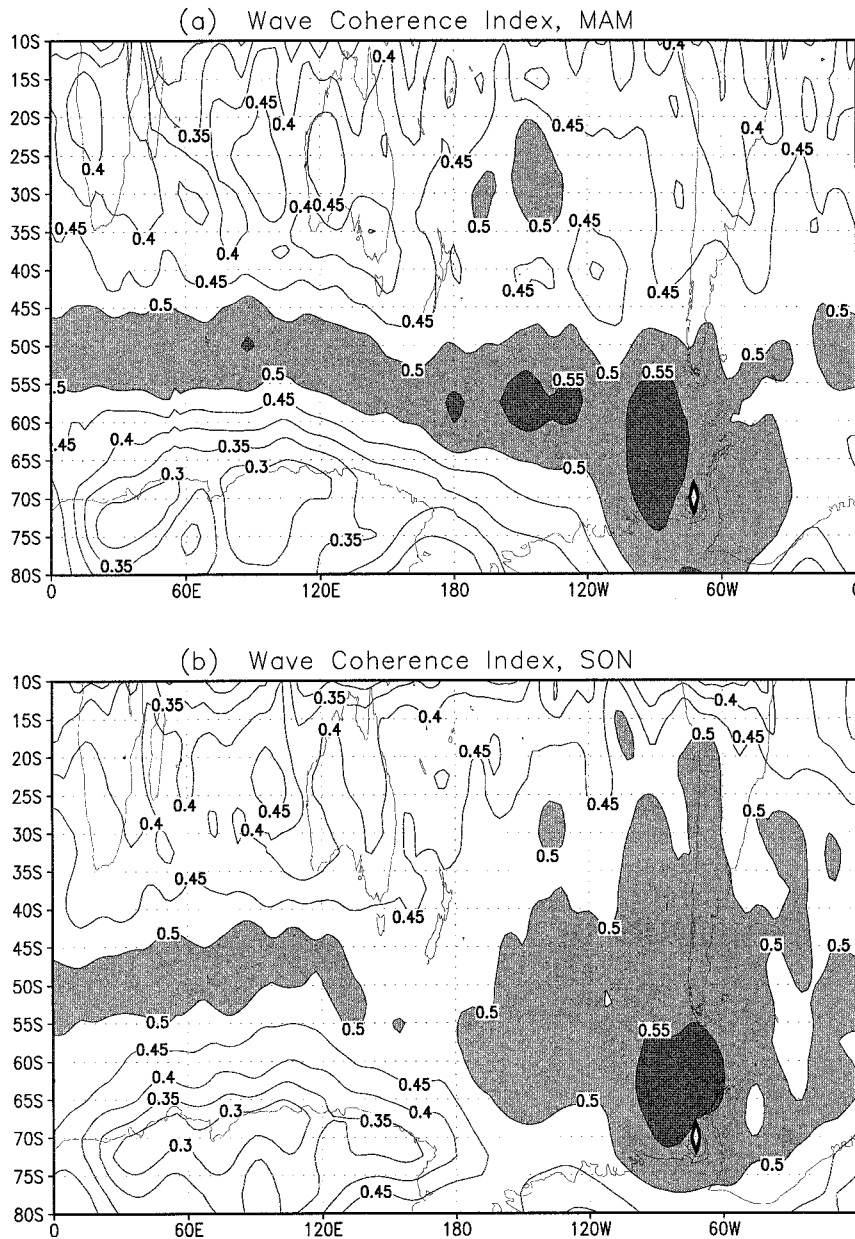


FIG. 5. Wave coherence index. Contour interval: 0.05. Shading represents values greater than 0.5.

in spring and autumn the wave train appears to split into two branches to the east of Australia propagating along the subtropical and subpolar jets. We have seen earlier (section 3a) that the split jet occurs in SON and MAM in a way similar to winter.

d. Characteristics of wave propagation in the transition seasons

The characteristics of wave propagation in JJA and DJF were discussed by C99. Here we examine wave propagation in the transition seasons SON and MAM

to identify similarities and differences. From Fig. 3 it can be seen that the zonal wind at 300 hPa shows a poleward spiral in MAM and SON. Thus it would be interesting to examine whether the wave packets propagate along such a spiral. For this we select a base point to the east of Australia in the middle of subtropical jet maximum. Figure 6a shows the lag correlation maps based on time series of v' at the base point (25°S , 165°E) for SON. Figure 6a for lags 2 and 4 shows poleward and eastward propagation of wave packets. The correlation coefficients are of lower magnitude in the figure for lag 4, and the wave propagation in this figure is less

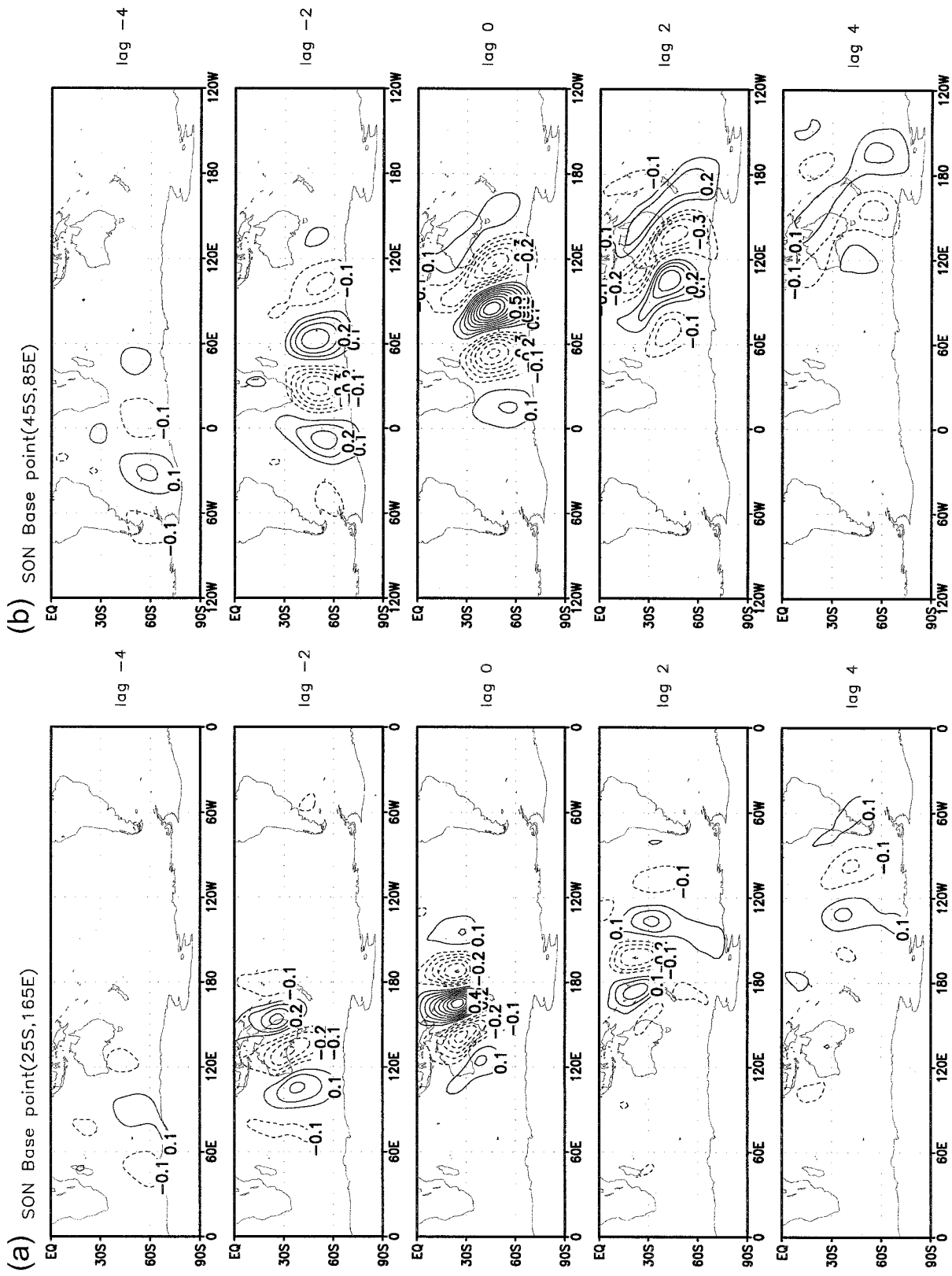


Fig. 6. (a) One-point lag correlation for SON v' at the base point 25°S, 165°E from day -4 to day +4. Contour interval: 0.1. Negative values are shown by broken lines.

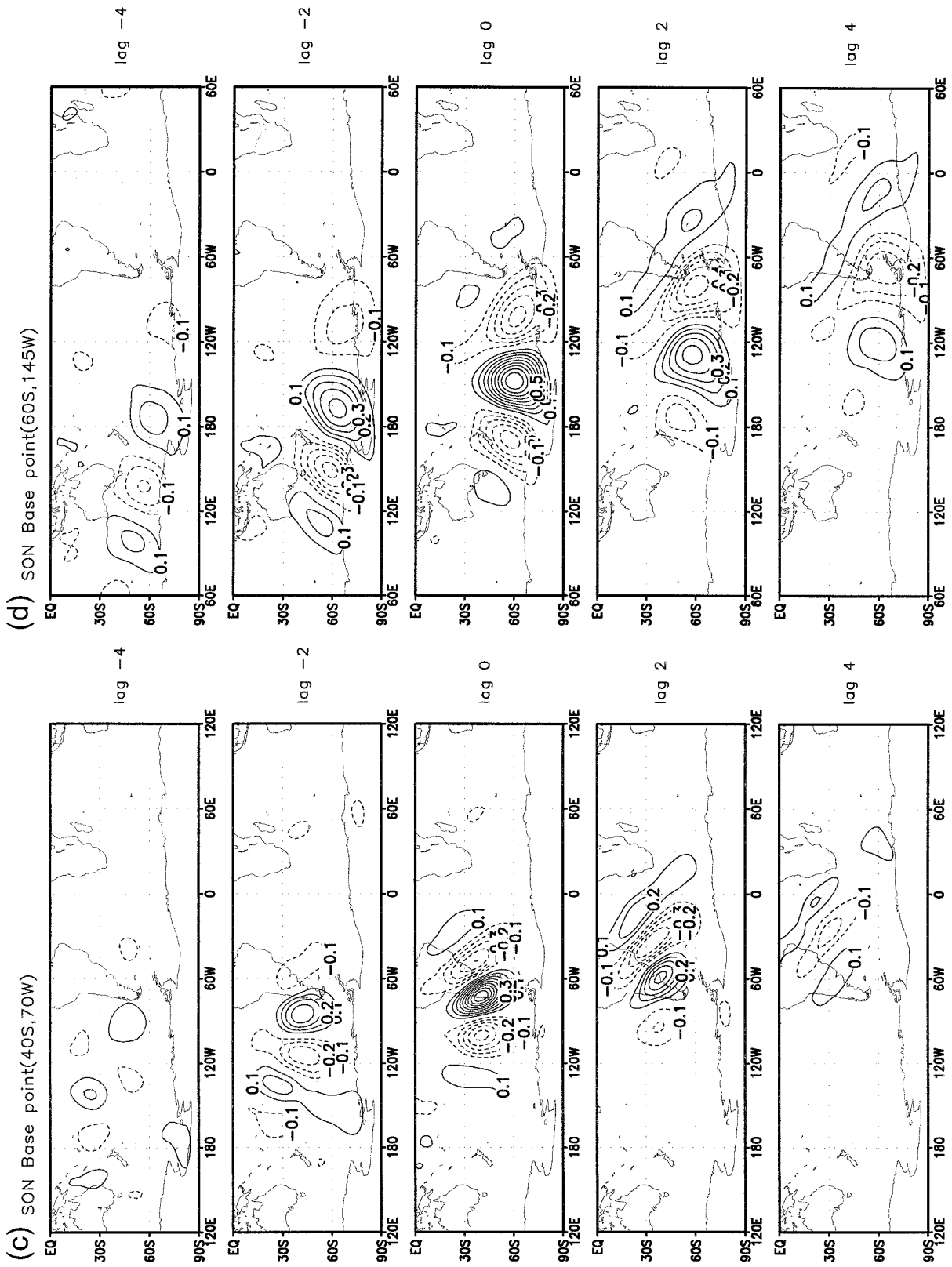


FIG. 6. (Continued) (b) Same as (a) but for the base point 45°S, 85°E. (c) Same as (a) but for the base point 40°S, 70°W. (d) Same as (a) but for the base point 60°S, 145°W.

clear compared to that noted by C99 for JJA. Figure 6a for lags -4 and -2 shows that in the upstream side wave packets move northward and eastward. More importantly, the waves that propagate through this base point seem to have propagated from southwest. However, the correlations in Fig. 6a for lag -4 are weaker.

Figure 6b for lags 0, 2, and 4 shows the situation on the downstream side of 45°S , 85°E . These figures suggest that the wave train splits into two branches to the east of 110°E , one branch propagating northeastward and the other southeastward. A close examination of figure for v_e in SON (not shown) shows, although less clearly than figure for winter, the split in the storm track east of Australia. Thus the split in the wave train to the east of Australia occurs also in spring similar to what was noted for JJA in C99. On the upstream side (Fig. 6b for lags -4 and -2), we can track the wave train toward the South Atlantic and South America.

Figure 6c shows the correlation maps for the base point 40°S , 70°W . As in the case of JJA (C99), the wave trains passing through this area have propagated from the subtropical jet stream. However, the magnitudes of the correlation coefficients are less in our case, and the number of centers of high correlation (positive or negative) are also less. This suggests that, although the characteristics of wave propagation are similar in JJA and SON, the propagation is less coherent in SON. Another interesting aspect of wave propagation seen in Fig. 6c for lags 2 and 4 is the tendency for the wave train to move equatorward on the lee side of Andes. In fact, Gan and Rao (1994) have suggested the role of Andes Cordillera in this type of wave propagation. Figure 6d shows the propagation of waves over the high-latitude branch of split jet. This figure shows the correlation maps for the base point 60°S , 145°W . It can be seen that the orientation of wave trains appears to be along the axis of the storm track. Thus a comparison of characteristics of our Figs. 6a, 6b, 6c, and 6d with those of C99 (his Figs. 10, 11, 12, and 13) shows that the wave propagation in SON is similar to that of JJA, although the wave propagation is less coherent (weaker correlation coefficients) in SON. In particular, the split in the wave propagation to the east of Australia occurs in SON also in a way similar to what happens in JJA. In order to take into account the seasonal shift of the general circulation, we repeated the analysis (figures not shown) with base points shifted 5° latitude to the pole compared to JJA. Essentially, the same results are obtained.

Figures 7a and 7b show, respectively, the correlation maps for MAM for the base points (25°S , 165°E) and (45°S , 85°E). The poleward spiral in the zonal wind (Fig. 3) can be seen in MAM in a way similar to SON, although the subtropical branch is less intense. Thus we selected the same base point as in the case of SON to verify wave propagation. From Fig. 7a at lag -4 , it can be seen that, just as in the case of JJA and SON, wave trains can be traced on the upwind side of this base point. Figure 7b is prepared to verify whether the split

in the wave train occurs in MAM in a way similar to what happens in SON. Indeed, the split in the wave train occurs to the east of about 110°E . One branch of the wave train seems to deviate northeastward into the subtropical jet stream and the other branch southeastward into the subpolar jet. Maps of correlation coefficients for the base points 40°S , 70°W and 60°S , 145°W for MAM (figures not shown) show characteristics similar to SON. We repeated calculations for DJF also (with long series of data), and the characteristics are similar to those noted in C99. Thus, our results for all the four seasons show that the split in the propagation of waves to the east of Australia occurs in MAM, JJA, and SON and not in DJF. In fact, a careful examination of the figure for v_e (figure not shown) shows that the split to the east of Australia shows a tendency to occur in all the seasons except summer.

There is a problem with NCEP–NCAR reanalysis data for the period 1980–1992. During this period PAOBS (SH bogus surface pressure observations produced by Australia) data were misplaced. Chang (2000) has shown that at the 300-hPa level (in our study the data are for this level) even in the presence of erroneous surface observations, the upper-air analysis of NCEP–NCAR is highly correlated with the ECMWF reanalysis, which does not suffer from this problem. However, we repeated the calculations with recent data for 1993–97 (which do not suffer the misplacement problem). The results confirm the split in the wave propagation in MAM, JJA, and SON to the east of Australia.

4. Summary and conclusions

In this paper we used 19 years (January 1979 through December 1997) of NCEP–NCAR reanalysis data to study the seasonal variations in the SH storm tracks and associated wave propagation. It is found that the SH storm track is strongest in MAM and weakest in SON. A time–latitude section of v_e also showed the autumn maximum and spring minimum. Most of the previous studies (C99; Berbery and Vera 1996) examined only summer (DJF) and winter (JJA) storm track characteristics. The present study, thus extends these previous studies, to the transition seasons.

The characteristics of wave packets are studied by computing 1-point lag correlation maps with the unfiltered meridional wind at 300 hPa. Here we extended C99's previous study of winter and summer by investigating all the four seasons.

The group velocity of the wave packets is determined by objectively tracking the movement of the centers of correlation obtained with v_e from day -1 to day $+1$. It is found that the group velocities are much higher than the phase velocities in all seasons. Thus, it can be concluded that the downstream development occurs throughout the year and so is a basic feature of upper-tropospheric waves in the midlatitudes of the SH. This extends the previous conclusions of C99 and Berbery

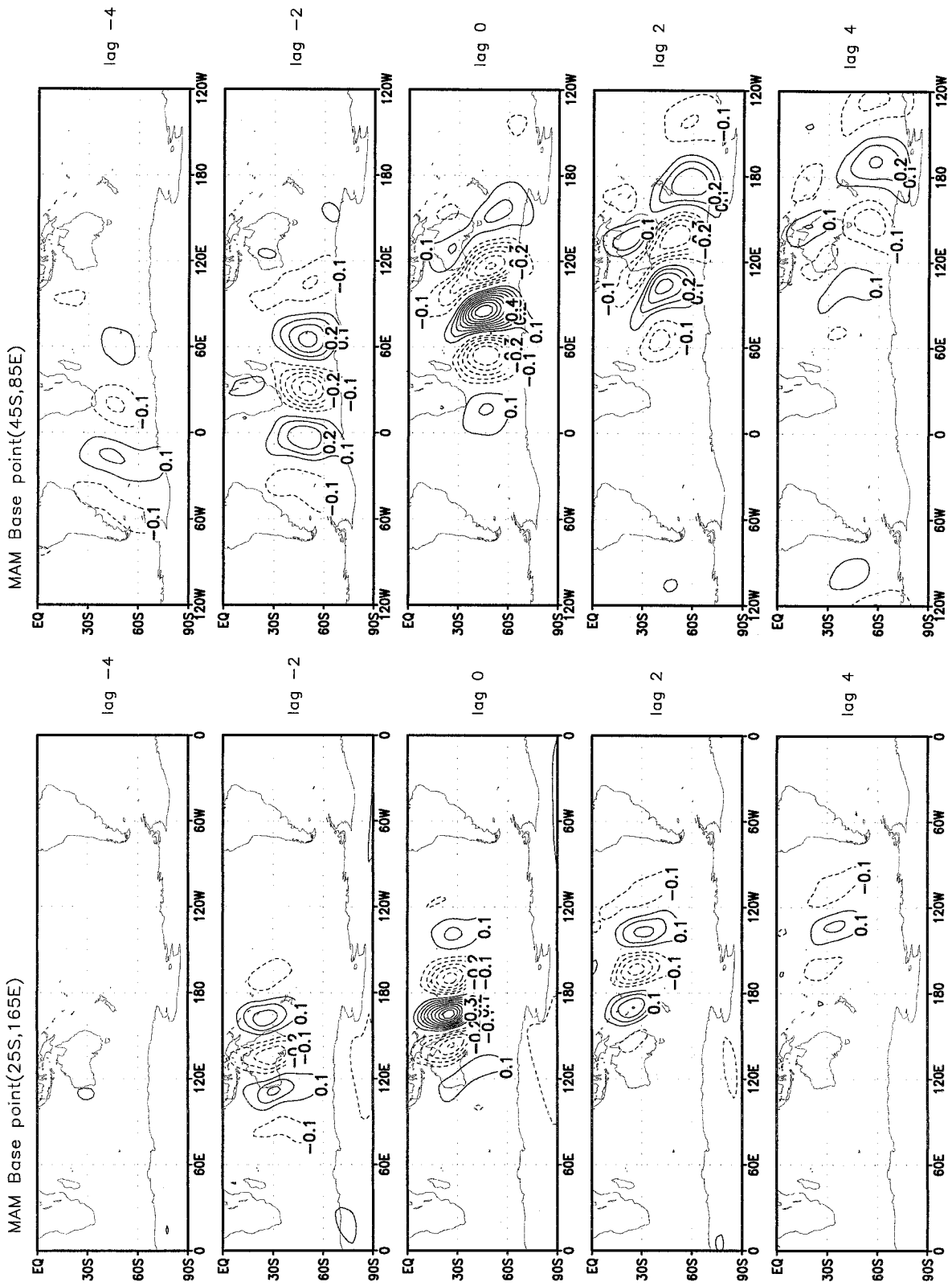


FIG. 7. Same as Fig. 6a but for MAM. (b) Same as Fig. 6a but for the grid point 45°S, 85°E.

and Vera (1996), who found downstream development in winter and summer seasons only.

Wave coherence defined as the average of the maximum (positive or negative) correlation upstream on day -2 and the downstream on day $+2$ is calculated for all the seasons. Based on this index and individual correlation maps the pathways in which the waves propagate preferentially can be inferred. The characteristics of the pathways or wave guides in winter and summer seasons are similar to what was found by C99.

In the present paper we extended the study of wave propagation to the transition seasons. We found that the wave propagation in spring is very similar to what happens in winter. In particular, the split of wave propagation to the east of Australia occurs also in spring in a way similar to what happens in winter. The split in the wave train occurs also in autumn to the east of Australia in a way similar to what happens in winter and spring. Thus, it can be concluded that the split in the wave train occurs to the east of Australia in all the seasons except summer.

Acknowledgments. Thanks are due to the two official reviewers whose suggestions led to substantial improvement of the paper. Thanks are also due to Dr. S. R. Chapa for critically going through the manuscript.

References

- Berbery, E. H., and C. S. Vera., 1996: Characteristics of the Southern Hemisphere winter storm track with filtered and unfiltered data. *J. Atmos. Sci.*, **53**, 468–481.
- Blackmon, M. L., 1976: A climatological spectral study of the 500 mb geopotential height of the Northern Hemisphere. *J. Atmos. Sci.*, **33**, 1607–1623.
- , J. M. Wallace, N.-C. Lau, and S. L. Mullen, 1977: An observational study of the Northern Hemisphere wintertime circulation. *J. Atmos. Sci.*, **34**, 1040–1053.
- , Y.-H. Lee, and J. M. Wallace, 1984a: Horizontal structure of 500 mb height fluctuations with long, intermediate and short time scales. *J. Atmos. Sci.*, **41**, 961–979.
- , —, —, and H.-H. Hsu, 1984b: Time variation of 500 mb height fluctuations with long, intermediate and short time scales as deduced from lag-correlation statistics. *J. Atmos. Sci.*, **41**, 981–991.
- Chang, E. K. M., 1993: Downstream development of baroclinic waves as inferred from regression analysis. *J. Atmos. Sci.*, **50**, 2038–2053.
- , 1999: Characteristics of wave packets in the upper troposphere. Part II: Seasonal and hemispheric variations. *J. Atmos. Sci.*, **56**, 1729–1747.
- , 2000: Wave packets and life cycles of troughs in the upper troposphere: Examples from the Southern Hemisphere summer season of 1984/85. *Mon. Wea. Rev.*, **128**, 25–50.
- , and I. Orlanski, 1993: On the dynamics of a storm track. *J. Atmos. Sci.*, **50**, 999–1015.
- , and D. B. Yu, 1999: Characteristics of wave packets in the upper troposphere. Part I: Northern Hemisphere winter. *J. Atmos. Sci.*, **56**, 1708–1728.
- Charney, J. G., 1947: The dynamics of long waves in a baroclinic westerly current. *J. Meteor.*, **4**, 135–162.
- Cressman, G. P., 1948: On the forecasting of long waves in the upper westerlies. *J. Meteor.*, **5**, 44–57.
- Eady, E. T., 1949: Long waves and cyclone waves. *Tellus*, **1**, 33–52.
- Frederiksen, J. S., and C. S. Frederiksen, 1993: Southern Hemisphere storm track, blocking, and low-frequency anomalies in a primitive equation model. *J. Atmos. Sci.*, **50**, 3148–3163.
- Gan, M. A., and V. B. Rao, 1994: The influence of the Andes Cordillera on transient disturbances. *Mon. Wea. Rev.*, **122**, 1141–1157.
- Hövmöeller, E., 1949: The trough-and-ridge diagram. *Tellus*, **1**, 62–66.
- Kalnay, E., and Coauthors, 1996: The NCEP/NCAR 40-Year Reanalysis Project. *Bull. Amer. Meteor. Soc.*, **77**, 437–471.
- Lau, N.-C., 1978: On the three-dimensional structure of the observed transient eddy statistics of the Northern Hemisphere wintertime circulation. *J. Atmos. Sci.*, **35**, 1900–1923.
- Lee, S., and I. M. Held, 1993: Baroclinic wave packets in models and observations. *J. Atmos. Sci.*, **50**, 1413–1428.
- Lim, G.-H., and J. M. Wallace, 1991: Structure and evolution of baroclinic waves as inferred from regression analysis. *J. Atmos. Sci.*, **48**, 1718–1731.
- Lorenz, E. N., 1955: Available potential energy and the maintenance of general circulation. *Tellus*, **7**, 157–167.
- Nakamura, H., and J. M. Wallace, 1990: Observed changes in baroclinic wave activity during the life cycles of low-frequency circulation anomalies. *J. Atmos. Sci.*, **47**, 1100–1116.
- Namias, J., and P. F. Clapp, 1944: Studies of the movement and development of long waves in the westerlies. *J. Meteor.*, **1**, 57–77.
- Orlanski, I., and J. Katzfey, 1991: The life cycle of a cyclone wave in the Southern Hemisphere. Part I: Eddy energy budget. *J. Atmos. Sci.*, **48**, 1972–1998.
- , and E. K. M. Chang, 1993: Ageostrophic geopotential fluxes in downstream and upstream development of baroclinic waves. *J. Atmos. Sci.*, **50**, 212–225.
- Randel, W. J., and J. L. Stanford, 1985: The observed life cycle of a baroclinic instability. *J. Atmos. Sci.*, **42**, 1364–1373.
- , and I. M. Held, 1991: Phase speed spectra of transient eddy fluxes and critical layer absorption. *J. Atmos. Sci.*, **48**, 688–697.
- Simmons, A. J., and B. J. Hoskins, 1978: The life cycle of some nonlinear baroclinic waves. *J. Atmos. Sci.*, **35**, 414–432.
- , and —, 1979: The downstream and upstream development of unstable baroclinic waves. *J. Atmos. Sci.*, **36**, 1239–1254.
- Trenberth, K. E., 1981: Observed Southern Hemisphere eddy statistics at 500 mb: Frequency and spatial dependence. *J. Atmos. Sci.*, **38**, 2585–2605.
- , 1982: Seasonality in Southern Hemisphere eddy statistics at 500 mb. *J. Atmos. Sci.*, **39**, 2507–2520.
- , 1991: Storm tracks in the Southern Hemisphere. *J. Atmos. Sci.*, **48**, 2159–2178.
- van Loon, H., 1965: A climatological study of the atmospheric circulation in the Southern Hemisphere during the IGY, Part I: 1 July 1957–31 March 1958. *J. Appl. Meteor.*, **4**, 479–491.
- Wallace, J. M., G.-H. Lim, and M. L. Blackmon., 1988: Relationship between cyclone tracks, anticyclone tracks, and baroclinic waveguides. *J. Atmos. Sci.*, **45**, 439–462.